Biophysical Journal
Article

Biophysical Society

Influence of Protein Scaffold on Side-Chain Transfer Free Energies

Dagen C. Marx[1] and Karen G. Fleming[1,*]
[1]Johns Hopkins University, Baltimore, Maryland

ABSTRACT The process by which membrane proteins fold involves the burial of side chains into lipid bilayers. Both structure and function of membrane proteins depend on the magnitudes of side-chain transfer free energies ($\Delta\Delta G^{o}_{sc}$). In the absence of other interactions, $\Delta\Delta G^{o}_{sc}$ is an independent property describing the energetics of an isolated side chain in the bilayer. However, in reality, side chains are attached to the peptide backbone and surrounded by other side chains in the protein scaffold in biology, which may alter the apparent $\Delta\Delta G^{o}_{sc}$. Previously we reported a whole protein water-to-bilayer hydrophobicity scale using the transmembrane β-barrel *Escherichia coli* OmpLA as a scaffold protein. To investigate how a different protein scaffold can modulate these energies, we measured $\Delta\Delta G^{o}_{sc}$ for all 20 amino acids using the transmembrane β-barrel *E. coli* PagP as a scaffold protein. This study represents, to our knowledge, the first instance of $\Delta\Delta G^{o}_{sc}$ measured in the same experimental conditions in two structurally and sequentially distinct protein scaffolds. Although the two hydrophobicity scales are strongly linearly correlated, we find that there are apparent scaffold induced changes in $\Delta\Delta G^{o}_{sc}$ for more than half of the side chains, most of which are polar residues. We propose that the protein scaffold affects the $\Delta\Delta G^{o}_{sc}$ of side chains that are buried in unfavorable environments by dictating the mechanisms by which the side chain can reach a more favorable environment and thus modulating the magnitude of $\Delta\Delta G^{o}_{sc}$.

INTRODUCTION

Membrane protein folding involves the burial of amino acid side chains in lipid bilayers (1). The favorability of this process can be quantified as a transfer free energy ($\Delta\Delta G^{o}_{sc}$) from water to lipid for each side chain (2,3). $\Delta\Delta G^{o}_{sc}$ values are used to predict transmembrane domains from protein sequences and, in theory, changes to membrane protein stability due to mutations (4,5). The accuracy of these predictions relies on the independence of measured side-chain transfer free energies from the protein scaffold where they are located and the experimental conditions in which they were determined. Although the scaffold independence of side-chain transfer free energies is always assumed, it has never been experimentally interrogated by measuring side-chain transfer free energies in different scaffolds in the same experimental conditions.

Previously, we developed a host-guest system that allowed for side-chain transfer free energies to be measured in the context of a natively folded protein in a lipid bilayer (6,7). Using this system, we measured side-chain transfer free energies for the center of the bilayer using the transmembrane β-barrel *Escherichia coli* outer membrane phospholipase A1 (OmpLA) as a scaffold protein (4). To assess the effects of protein scaffold on side-chain transfer free energies we have extended our host-guest system to a new scaffold protein: the transmembrane β-barrel outer-membrane acyl transferase PagP from *E. coli*. As a scaffold, PagP is structurally distinct from OmpLA in a variety of ways, including the number of transmembrane β-strands, the tilt of the β-barrel with respect to the bilayer, and the amino acid composition of the transmembrane domain (8–12). In an effort to be consistent with the previously measured whole-protein hydrophobicity scale, we have chosen a host site on PagP that is predicted to be in a central and nonpolar region of the lipid bilayer. By measuring the $\Delta\Delta G^{o}_{sc}$ at approximately the same depth in the bilayer and using the same experimental conditions as used previously, we can directly parse out the effects imparted on side chains by the scaffold protein.

We find that the PagP hydrophobicity scale correlates very well with the OmpLA hydrophobicity scale, especially for nonpolar residues. For polar residues, we find energetic differences between the two proteins, with residues consistently more favorable in PagP than in OmpLA. These

Submitted April 7, 2017, and accepted for publication June 19, 2017.
*Correspondence: karen.fleming@jhu.edu
Editor: Charles Deber.
http://dx.doi.org/10.1016/j.bpj.2017.06.032

discrepancies are rationalized as both local- and global-difference scaffold properties that alter $\Delta\Delta G^{o}_{sc}$. These findings highlight the intricacies of not only membrane protein folding, but also the influence of individual side-chain packing on the overall stability of membrane proteins.

MATERIALS AND METHODS

PagP expression, purification, and chemical denaturation titrations

The methods for protein cloning and purification, as well as the experimental procedures, are identical to previously published protocols (4,13,14). Briefly, wild-type (WT) PagP was previously cloned into a pET11A plasmid. PagP variants were cloned using the In-fusion HD cloning kit by Clonetech (Mountain View, CA) as described by the manufacturer, except for V111C, which was cloned by Genewiz (South Plainfield, NJ). Plasmids were transformed into hms174(DE3) cells via electroporation and sequenced by Genewiz. Cells were grown in 500 mL TB until OD_{600nm} reached 0.8–1.0 and were induced with 1 mM isopropyl-β-D-1-thiogalactopyranoside (IPTG) before growing for 6 h. Cells were harvested by centrifugation at 5000 Rpm for 15 min and stored at −20°C overnight.

Cell pellets were suspended in 25 mL lysis buffer (50 mM Tris, and 40 mM EDTA (pH 8.0)). Cells were lysed using Avestin (Ottawa, Canada) emulsiflex C3 at 15,000 psi. Brij-L23 detergent was added at 0.1% before inclusion bodies (IBs) were harvested via ultracentrifugation at 5500 Rpm for 30 min, discarding the supernatant. IB pellets were suspended and pelleted two more times in wash buffer (10 mM Tris and 1 mM EDTA (pH 8.0)) to wash out any contaminating, soluble macromolecules. Finally, IBs were suspended in 10 mL wash buffer and aliquoted into 10 USA Scientific microcentrifuge tubes. IBs were pelleted at 13.3 Rpm for 5 min on a tabletop centrifuge and stored at −20°C after the supernatant was removed.

Before solubilization, IBs were suspended with 1 mL titration buffer (100 mM citrate and 2 mM EDTA (pH 3.8)), split into two microcentrifuge tubes, and pelleted at 13.3 Rpm for 5 min. Inclusion bodies were solubilized in 8 M guanidine hydrochloride titration buffer. The remaining insoluble contaminants were pelleted at 13.3 Rpm for 20 min and the supernatant was filtered with a 0.22 μm filter. Final protein concentration before folding proteins into LUVs was adjusted to $\leq$100 μM.

1,2-dilauroyl-*sn*-glycero-3-phosphocholine (DLPC) lipids were purchased from Avanti Polar Lipids (Alabaster, AL) and aliquoted into acid washed glass vials at 25 mg/vial using Hamilton syringes. Lipids were dried with nitrogen gas before being put in a freeze dryer overnight and stored at −20°C under nitrogen. Lipids were solubilized to a concentration of 25 mg/mL in titration buffer. LUVs were formed via extrusion through a 0.1 μm filter 21 times using an Avanti mini-extruder.

The procedure for folding PagP into LUVs was previously described and follows the procedure described for measuring OmpLA folding, but using the extinction coefficient of 82,360 M-1 for PagP in 6 M guanidine hydrochloride (GdnHCl) (14). Briefly, protein was diluted to 6 μM in the presence of SB3-14 detergent (Sigma-Aldrich, St. Louis, MO) in 2.5 M GdnHCl. Protein was then diluted to a protein/lipid ratio of 1:2000 in either 2.5 or 5 M GdnHCl for unfolding and folding titrations, respectively. These samples were then incubated overnight at 37°C in a rotating incubator at 6 Rpm. Samples were then finally diluted to 400 nM protein concentration in microcentrifuge tubes at a range of GdnHCl concentrations (2–6 M) and incubated for a minimum of 40 h at 37°C in the rotating incubator.

Folding and unfolding of PagP was monitored via intrinsic tryptophan fluorescence. All fluorescence experiments were collected on an ISS (Champaign, IL) PC1 photon counting fluorometer with excitation polarizer at 90° with 2.4 mm slits, emission polarizer at 0° with 2.0 mm slits, and pathlength of 1 cm. For reversibility determination titrations, wavelength scans were collected (λ_{ex} = 295 nm, λ_{em} = 280–400 nm) twice for each sample. Full-wavelength scans were fit to a log-normal function, as previously described. To determine PagP variant stabilities, 100 readings of emission intensity were recorded at each concentration of GdnHCl (λ_{ex} = 295 nm, λ_{em} = 330 nm). Three independent titrations of each PagP variant were collected.

To determine $\Delta G^{o}_{w,l}$ for all PagP variants, we globally fit all titrations to a two-state linear extrapolation model using Igor Pro (Wavemetrics, Lake Oswego, OR). We determined a singular *m*-value that best described all PagP variants (m = 4.97), which was slightly different from the previously determined m-value for WT PagP (14).

Molecular dynamics simulations of PagP variants

We used all-atom molecular dynamics (MD) simulations to investigate the structural consequences of the V111P PagP variant. Systems were constructed using PDB: 1mm4 as the starting structure of PagP (1MM4) aligned by the Orientation of Proteins in Membranes database (12,15). CHARMM-GUI was used to build the systems and generate equilibration and production files (16–20). Two WT PagP and two V11P systems were generated with homogeneous DLPC bilayers and 0.2 M NaCl. To approximate the pH of the experimental system (3.8), we protonated all histidine residues in PagP and left all Glu and Asp deprotonated. We chose to adopt this protocol because pH 3.8 is close to the model-compound pKa values of Glu and Asp side chains, so that accurately predicting the protonation states of these residues is challenging. Additionally, Glu and Asp residues in PagP are confined almost exclusively to soluble regions of the protein, and should not affect the barrel conformation near the site of mutation.

Simulations were equilibrated using the CHARMM-GUI equilibration protocol. Trajectory 1 for both WT and V111P PagP were initially run at 30°C for 200 ns. The temperature in the two systems was then slowly increased to 37°C to match the experimental temperature. These systems were run for 110 ns more, of which the final 100 ns was used in analysis. Trajectory 2 for both WT and V111P PagP were run using nanoscale MD at 37°C for the entire simulation, again using the final 100 ns for analysis. Fig. S1 shows that all trajectories equilibrated well before the final 100 ns used for analysis of the protein. All simulations were run on the Maryland Advanced Research Computing Center super computer. Analysis of the MD simulations was performed using a combination of VMD plug-ins and homemade scripts. To determine the effect of the V111P variant we measured distances between the proposed backbone hydrogen bonding atoms (carbonyl-carbon and nitrogen) in residues 111 and 85 for the last 100 ns.

RESULTS AND DISCUSSION

PagP hydrophobicity scale at site 111

We utilized a previously developed host-guest system to measure $\Delta\Delta G^{o}_{sc}$ in which all residues are substituted into a chosen host site on PagP (4,13). Fig. 1 shows the location of the host site, residue 111 (valine in WT PagP), which is located at the end of the fifth strand of the transmembrane β-barrel. The nearest-neighbor residues at this site are predominately hydrophobic (proline and alanine), with a tyrosine hydroxyl group as the lone source of polarity. As such, the host site on PagP is chemically very similar to the host site on OmpLA, yet it is composed of distinct residues. The z-distance from the bilayer center to the Cα for this site on PagP is predicted to be 5 Å, which differs from the host site on OmpLA, which was calculated to be 0.4 Å (8,11,21). However, previous calculations of the depth-dependent atomic composition of symmetric DLPC bilayers

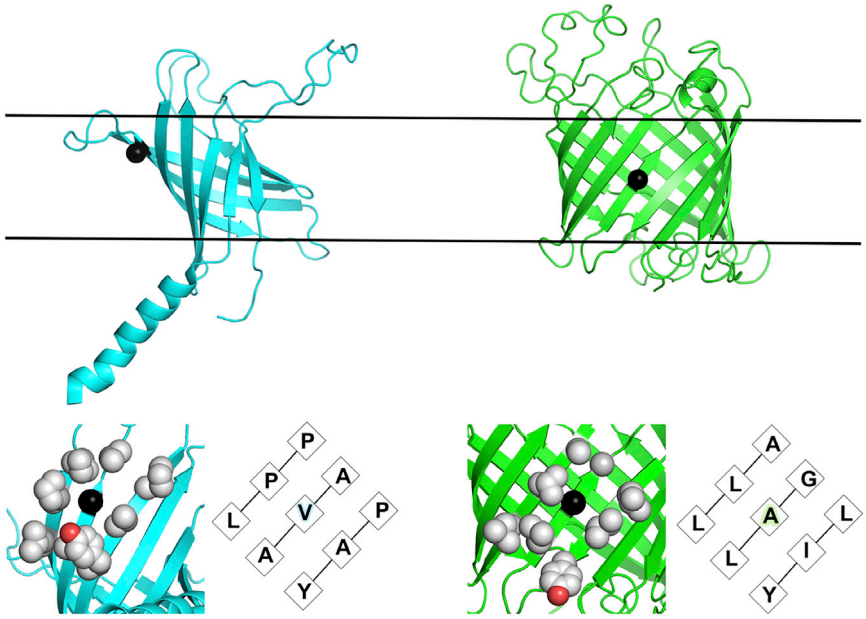

FIGURE 1 Comparison of structural characteristics of PagP and OmpLA. PagP (PDB: 1MM4) (*left*) is colored in cyan and has eight transmembrane β-strands and a periplasmic helix. OmpLA (PDB: 1QD5) (*right*), colored green, has 12 transmembrane strands and is not tilted with respect to the bilayer (shown as *black lines*). Sites at which transfer free energies were measured are shown as black spheres (PagP V111 and OmpLA A210), highlighting the different depths of the two positions. Shown below the structures are the nearest-neighbor residues of the sites mutated in the two studies (shown in *black spheres*). This figure was created using PyMOL (33). To see this figure in color, go online.

found that the bilayer is essentially chemically identical within ± 5 Å from the bilayer center (13). Additionally, side chains at site 111 extend toward the hydrophobic membrane center due to the tilt of the PagP barrel. Thus, the $\Delta\Delta G^{o}_{sc}$ measured in PagP can be directly compared to those previously determined in OmpLA, because the side chains are predicted to experience chemically identical regions of the bilayer. Because our host-guest system requires alanine to be the host residue, PagP V111A is the host protein that is used in all calculations. All other amino acids were individually substituted into this site as guest residues.

To extract thermodynamic quantities from folding titrations, PagP must fold spontaneously via a path-independent mechanism. WT PagP folding into DLPC large unilamellar vesicles (LUVS) has been previously shown to meet these requirements at pH 3.8 (14). Fig. 2 shows our verification

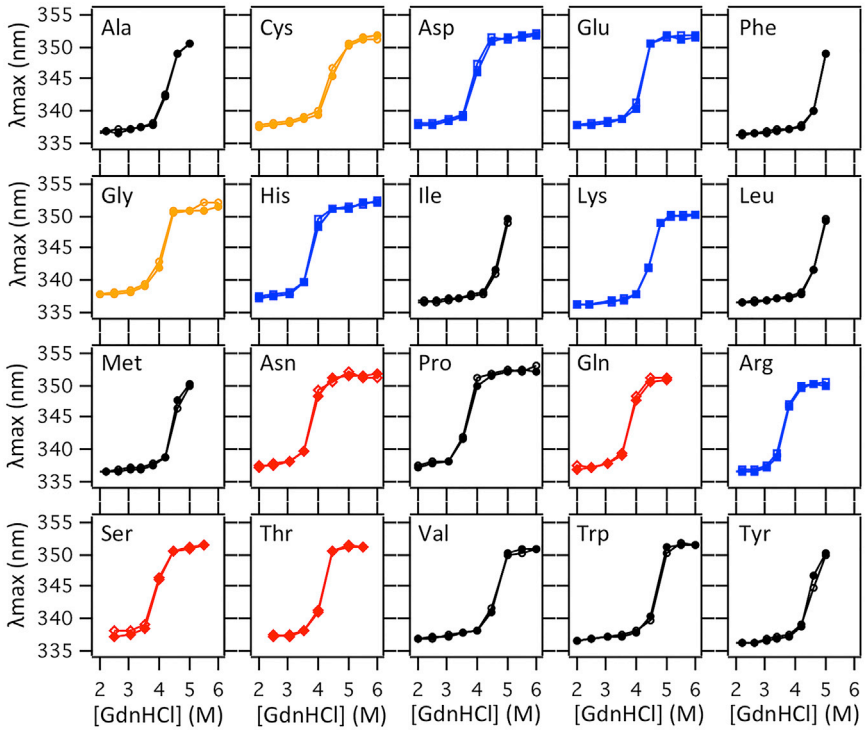

FIGURE 2 All PagP variants show path independence in chemical denaturation titrations. Unfolding titrations are shown by open symbols and overlaid upon folding titrations, which are shown by solid symbols. The variant is noted in each box, and the coloring scheme is identical to that in Fig. 3 and Fig. S1. To see this figure in color, go online.

that all variants met these requirements using intrinsic tryptophan fluorescence, and Fig. 3 shows representative high-resolution titration data demonstrating excellent fits by the two-state linear extrapolation equation, allowing for the stability in the absence of denaturant ($\Delta G^{o}_{w,l}$) to be calculated for each variant (22,23). These experimentally observed values are reported in Table 1. By taking the difference in $\Delta G^{o}_{w,l}$ of the PagP host variant (Ala) and a PagP guest variant we can determine the transfer free energy ($\Delta\Delta G^{o}_{w,l}$) of the guest side chain into the center of the bilayer with respect to alanine (4,13).

The resultant $\Delta\Delta G^{o}_{w,l}$ values for all side chains are shown in Fig. S1 and Table 1, where it can be observed that nonpolar and aromatic side-chain substitutions are stabilizing to native PagP in bilayers. In contrast, ionizable and polar residues destabilized PagP structure. Given the highly hydrophobic composition of the DLPC bilayer around the host site, the burial of hydrophobic residues was expected to be favorable, whereas hydrophilic residues were expected to be unfavorable.

Nonpolar side-chain burial at the membrane center is scaffold independent

For transfer free energies to be applied generally in predictive algorithms, the transfer free energy for each residue should be an independent value. To remove the dependence of $\Delta\Delta G^{o}_{w,l}$ on the stability of the host protein (V111A), we calculated the nonpolar solvation parameter (σ_{NP}) for our host site in PagP (24,25). Because σ_{NP} describes the linear correlation between buried nonpolar surface area and transfer free energy, it can be used to calculate the theoretical $\Delta\Delta G^{o}_{w,l}$ for alanine.

We used the experimental data for the nonpolar side chains to derive σ_{NP} for PagP at site 111. Shown in Fig. 4, this analysis revealed a robust linear correlation between aliphatic side-chain energetic perturbations and nonpolar accessible surface area in an extended G-X-G tripeptide ($R^2 = 0.91$). The slope reveals the magnitude of σ_{NP} to equal 25 cal^{-1} mol^{-1} Å^{-2} for transfer of nonpolar surface area from the membrane to water. This PagP σ_{NP} is almost identical to that observed in OmpLA (23 cal^{-1} mol^{-1} Å^{-2}) for a comparable depth in the bilayer (4). Therefore, we find that the energy associated with nonpolar side-chain burial in the center of the membrane is mostly independent of both local side-chain packing and side-chain orientation with respect to the membrane normal. Additionally, the PagP σ_{NP} is easily within the range of σ_{NP} measured in other contexts, such as hydrophobic solvents, α-helical membrane proteins, or statistical analyses of the interiors of soluble proteins, highlighting the robustness of our host-guest system (24–27).

We used the nonpolar accessible surface area of the alanine side chain in a G-X-G peptide and this σ_{NP} to calculate the water-to-bilayer energy of alanine at our host site ($\Delta\Delta G^{o}_{w,l} = -1.73$ kcal mol^{-1}). Adding this energy change

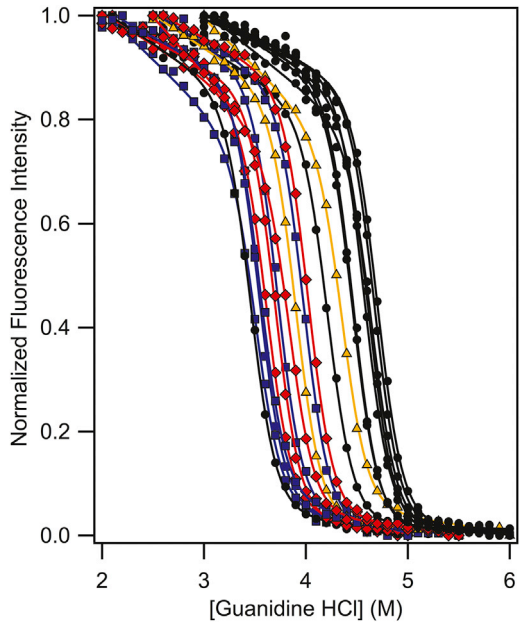

FIGURE 3 High-resolution chemical denaturation titrations of PagP variants. Representative chemical denaturation titration data for all 20 PagP variants at position V111 with ionizable residues colored blue, polar residues red, nonpolar residues black, and cysteine and glycine in gold. Normalized intrinsic tryptophan fluorescence intensity is plotted as a function of the concentration of guanidine HCl. Data were fit to a two-state folding model with the *m*-value held constant ($m = 4.97$). To see this figure in color, go online.

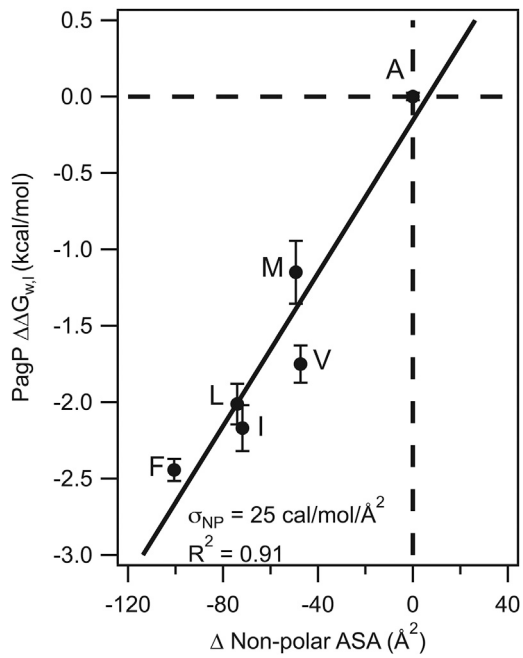

FIGURE 4 Determination of the nonpolar solvation parameter at PagP site 111. The $\Delta\Delta G^{o}_{w,l}$ values of nonpolar residues were plotted as a function of their nonpolar accessible surface area in a G-X-Gly tripeptide, where X is any amino acid. The correlation is well described ($R^2 = 0.91$), with intercept equal to 0.156 and slope equal to 25 cal mol^{-1} A^{-2}, which reflects the value of the σ_{NP} from bilayer to water.

TABLE 1 Values for Stabilities and Transfer Free Energies

Variant	Experimentally Observed $\Delta G^{o}_{w,l}$ [a] (kcal mol^{-1})	Difference between V111A and Variant $\Delta\Delta G^{o}_{w,l}$ [b] (kcal mol^{-1})	Reference-Free Side-Chain Energies $\Delta\Delta G^{o}_{sc}$ [c] (kcal mol^{-1})	Difference between PagP and OmpLA $\Delta\Delta\Delta G^{o}_{sc}$ [d] (kcal mol^{-1})
V111A	−20.96 ± 0.02	0.00 ± 0.02	−1.73 ± 0.02	−0.16 ± 0.02
V111C	−21.69 ± 0.03	−0.72 ± 0.04	−2.45 ± 0.04	−1.37 ± 0.15
V111D	−18.47 ± 0.09	2.49 ± 0.09	0.77 ± 0.09	−0.61 ± 0.20
V111E	−19.78 ± 0.14	1.18 ± 0.14	−0.54 ± 0.14	−0.61 ± 0.19
V111F	−23.41 ± 0.07	−2.44 ± 0.07	−4.17 ± 0.07	−0.40 ± 0.28
V111G	−19.32 ± 0.10	1.64 ± 0.11	−0.09 ± 0.11	−0.24 ± 0.16
V111H	−17.64 ± 0.12	3.32 ± 0.12	1.60 ± 0.12	−1.59 ± 0.28
V111I	−23.13 ± 0.15	−2.17 ± 0.15	−3.90 ± 0.15	−0.78 ± 0.38
V111K	−17.43 ± 0.08	3.54 ± 0.08	1.81 ± 0.08	−2.01 ± 0.53
V111L	−22.98 ± 0.13	−2.01 ± 0.13	−3.74 ± 0.13	−0.42 ± 0.19
V111M	−22.11 ± 0.20	−1.15 ± 0.21	−2.88 ± 0.21	−0.55 ± 0.28
V111N	−18.02 ± 0.03	2.95 ± 0.03	1.22 ± 0.03	−0.69 ± 0.28
V111P	−17.15 ± 0.07	3.82 ± 0.07	2.09 ± 0.07	5.18 ± 0.14
V111Q	−18.43 ± 0.03	2.54 ± 0.03	0.81 ± 0.03	−0.63 ± 0.11
V111R	−17.75 ± 0.06	3.22 ± 0.06	1.49 ± 0.06	−0.65 ± 0.14
V111S	−19.13 ± 0.03	1.83 ± 0.04	0.11 ± 0.04	−0.15 ± 0.22
V111T	−20.02 ± 0.05	0.95 ± 0.05	−0.78 ± 0.05	−0.99 ± 0.34
WT (V)	−22.71 ± 0.12	−1.75 ± 0.12	−3.48 ± 0.12	−1.14 ± 0.31
V111W	−23.17 ± 0.01	−2.21 ± 0.02	−3.93 ± 0.02	−1.98 ± 0.21
V111Y	−21.99 ± 0.28	−1.02 ± 0.28	−2.75 ± 0.28	−0.09 ± 0.30

Errors are standard deviations from $n = 3$ independent measurements.
[a]$\Delta G^{o}_{w,l}$ values correspond to the Gibbs free energy of folding of each variant from water (w) to the lipid bilayer (l) extrapolated to the absence of denaturant. A folding free energy m-value of −4.97 kcal mol^{-1} M^{-1} was determined as a global parameter by simultaneous fitting of all data in this study (Fig. 3 *A*).
[b]$\Delta\Delta G^{o}_{w,l}$ values correspond to water-to-lipid free-energy perturbations introduced by each mutation relative to the alanine variant (shown in Fig. S1 *B*).
[c]$\Delta\Delta G^{o}_{sc}$ values correspond to side-chain energetic perturbations. These are reference-free values that have had the dependence of alanine removed by calculating the theoretical $\Delta\Delta G^{o}_{sc}$ of alanine using the nonpolar solvation parameter. The energies of all other side chains are adjusted by the new alanine energy (shown in Fig. 5 *B*).
[d]$\Delta\Delta\Delta G^{o}_{sc}$ values correspond to the difference between $\Delta\Delta G^{o}_{sc}$ measured at site 111 in PagP and those measured at site 210 in OmpLA. Negative numbers indicate that $\Delta\Delta G^{o}_{sc}$ values were more favorable (more negative) in PagP than in OmpLA. Positive numbers indicate that $\Delta\Delta G^{o}_{sc}$ values were more favorable when measured in OmpLA. Errors were propagated from $\Delta\Delta G^{o}_{sc}$.

to those of all side chains effectively shifts the set of measurements to a reference-free form. Fig. 5 and Table 1 show these values ($\Delta\Delta G^{o}_{SC}$), which can be interpreted as side-chain water-to-bilayer hydrophobicity values for all amino acid side chains.

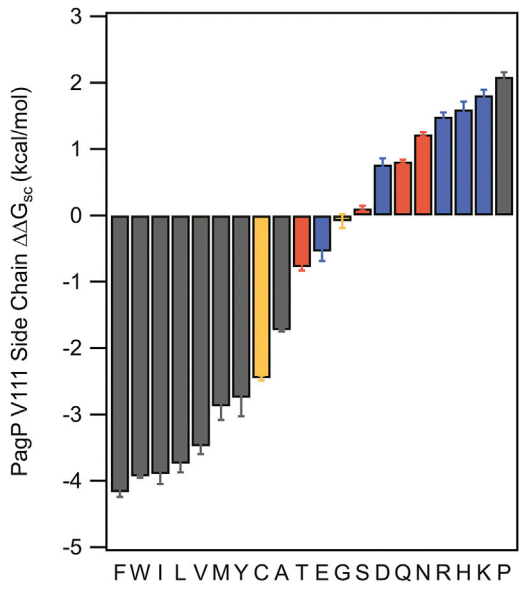

FIGURE 5 Reference-free $\Delta\Delta G^{o}_{sc}$ values for all side chains. Side-chain transfer free energies for all 20 amino acids at site 111 after correcting for the transfer free energy of alanine. Error bars are standard deviations ($n = 3$ for all variants). To see this figure in color, go online.

Proline-induced secondary structure disruption is energetically equivalent in α-helices and β-barrels

By comparing the $\Delta\Delta G^{o}_{SC}$ measured in PagP and OmpLA we can obtain a sense of the scaffold dependence of transfer free energy measurements of individual side chains. The biggest discrepancy between the two hydrophobicity scales is proline, which is the most destabilizing mutation in this investigation, but was found to be favorable in previous measurements ($\Delta\Delta\Delta G^{o}_{SC} = +5.18 \pm 0.14$ kcal mol^{-1}) (4). This large difference in $\Delta\Delta G^{o}_{SC}$ between the two studies highlights the magnitude to which factors other than solvation can influence the transfer free energy of a given side chain.

To investigate the molecular origins of the scaffold dependence of proline $\Delta\Delta G^{o}_{SC}$, we performed MD simulations on both the PagP proline variant (V111P) and WT PagP in a DLPC bilayer. Because site 111 is at the end of a β-strand, we hypothesized that this location affects the energetic outcome through a mechanism independent of simple solvation. Indeed, proline is rarely found in secondary structure because of severe limitations on backbone torsion and the removal of a backbone hydrogen-bond donor

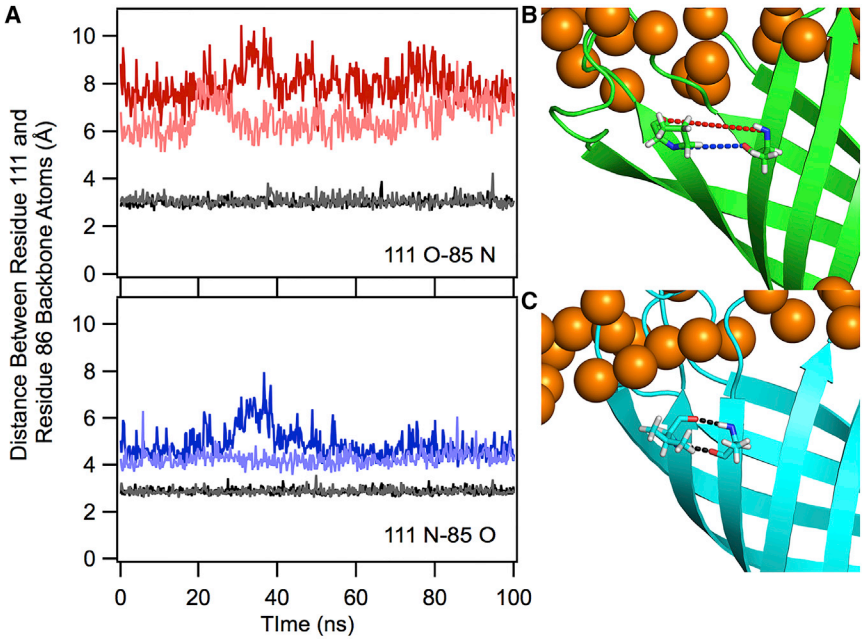

FIGURE 6 V111P induces local unfolding in PagP. (*A*) To assess the effect of the V111P variant on PagP structure we measured the distance between the backbone hydrogen-bonding atoms between residues 111 and 85. The top panel shows the distance between the carbonyl oxygen on residue 111 and the backbone nitrogen of residue 85, with the two WT trajectories colored gray and V111P trajectories colored red. The bottom panel shows the distance between the residue 111 backbone nitrogen and the residue 85 carbonyl oxygen, with WT PagP trajectories colored gray and V111P trajectories colored blue. The distances in V111P are too large for any contacts between the residues indicating a local unfolding event. (*B*) Snapshot from V111P trajectory showing the local unfolding of the β-sheet. The coloring scheme from (*A*) is used to show the two different distances being measured. (*C*) Snapshot from the WT trajectory showing close contacts between residues 111 and 85. (*B*) and (*C*) were created using PyMoL, and DLPC phosphates are shown as orange spheres in both images (33). To see this figure in color, go online.

(28,29). Although the exposure of backbone polar atoms can be accommodated in soluble proteins through interactions with solvent, the center of the membrane lacks polar atoms to satisfy side backbone hydrogen-bonding requirements. In WT PagP, residue 111 forms backbone hydrogen bonds with residue 85 in the neighboring strand (11,12). To determine the effect of the V111P mutation on the structure of PagP we measured the distances between backbone nitrogen and carbonyl carbon atoms of residues 111 and 85 in both WT and V111P in multiple, independently seeded trajectories (30).

We found that the distances in V111P increase substantially compared to WT PagP, resulting in a break in secondary structure leading to local fraying of the ends and a localized unfolding event, which is not observed in the WT PagP trajectories (Fig. 6). Thus, we find that the exposure of multiple polar backbone atoms combined with other local unfolding events is the likely cause of the unfavorable $\Delta\Delta G^{o}_{SC}$ for proline in PagP. We hypothesize that the host position in OmpLA can accommodate the torsion angle strain induced by proline because it is in the center of a strand rather than near the end of a strand, thus only breaking one transmembrane backbone hydrogen bond. Additionally, the larger OmpLA has more water in the center of the transmembrane barrel, which may hydrogen bond with the exposed polar backbone atoms. Given estimates of a 4–5 kcal/mol penalty for breaking a hydrogen bond in the membrane, a simple interpretation of the $\Delta\Delta\Delta G^{o}_{SC}$ for proline could be that PagP V111P breaks an extra hydrogen bond compared to OmpLA A210P (3). Interestingly, the energetic cost for proline in PagP is almost identical to transfer free energies measured for proline insertion in the middle of transmembrane α-helices, implying that the energetic cost of proline-induced structural deformations may be independent of secondary structure type (29,31).

Comparison with OmpLA hydrophobicity scale reveals scaffold dependence of $\Delta\Delta G^{o}_{SC}$

With the exclusion of proline, the PagP and OmpLA hydrophobicity scales are strongly linearly correlated (Fig. 7). However, the slope of the correlation is not equal to 1

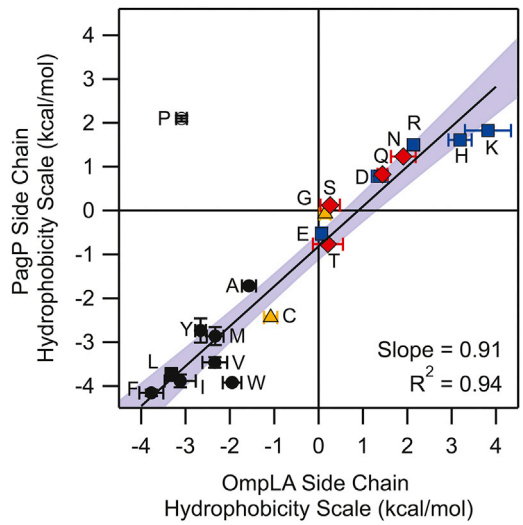

FIGURE 7 PagP and OmpLA hydrophobicity scales are well correlated. The plot shows the comparison of the two whole-protein water-to-bilayer hydrophobicity scales with PagP on the *y* axis and OmpLA on the *x* axis. Residues are colored with the same coloring scheme as in Fig. 2. The 95% confidence intervals of the fit are shown in light blue. Proline was excluded from the linear fit and subsequent determination of confidence intervals. To see this figure in color, go online.

(slope = 0.91 ± 0.05), suggesting that $\Delta\Delta G^{o}_{SC}$ for all side chains is not completely scaffold independent. In addition, the intercept is −0.83, indicating a context dependence of $\Delta\Delta G^{o}_{SC}$. We find that all side chains, except proline, have more favorable $\Delta\Delta G^{o}_{SC}$ values when measured in the PagP scaffold than when measuared in OmpLA, though the magnitude of the difference in $\Delta\Delta G^{o}_{SC}$ ($\Delta\Delta\Delta G^{o}_{SC}$) varies (Table 1). Because we find that this trend applies for every side chain, general properties of the PagP structure must be contributing to the negative $\Delta\Delta\Delta G^{o}_{SC}$. Given the known structural differences, we hypothesize that the decreased strand number changes the overall density of side chain packing slightly and may increase side-chain entropy or side-chain contacts with lipid acyl tails, resulting in $\Delta\Delta G^{o}_{SC}$ that are more favorable in PagP.

For most nonpolar and aromatic residues we find $\Delta\Delta\Delta G^{o}_{SC}$ is <0.5 kcal mol^{-1}, suggesting that the differences between PagP and OmpLA are marginal for these residues (A, F, L, M, and Y) and that $\Delta\Delta G^{o}_{SC}$ is generally independent of the scaffold in which they were measured. This is unsurprising given the similar σ_{NP} determined for PagP and OmpLA. We find that this scaffold independence also holds for glycine and serine. $\Delta\Delta\Delta G^{o}_{SC}$ for all other residues is >0.5 kcal mol^{-1}, which indicates that some prominent local or global difference between the two scaffold proteins is altering the magnitude of $\Delta\Delta G^{o}_{SC}$.

We find a $\Delta\Delta\Delta G^{o}_{SC}$ of ∼−1 kcal mol^{-1} for the β-branched residues isoleucine, threonine, and valine (Table 1). We attribute this difference in $\Delta\Delta G^{o}_{SC}$ to the evolved local side-chain packing in each scaffold for the WT residues in each host site. Because the WT residue at the PagP host site is valine, we hypothesize that PagP has evolved favorable contacts between nearest-neighbor residues and branched β-carbons at site 111. This contrasts with OmpLA, which has an alanine at the host site 210, and therefore would not have evolved favorable interactions for β-branched residues at that site.

The remaining residues that exhibit apparent scaffold dependence for $\Delta\Delta G^{o}_{SC}$ all contain polar atoms, with $\Delta\Delta\Delta G^{o}_{SC}$ ranging from −0.6 to −2.0 kcal mol^{-1}. Mechanistically, solvation of polar residues in the membrane is accomplished in two ways: side chain "snorkeling" from the center of the bilayer to the interface, and the formation of lipid defects such as water dimples (8). Although we initially thought that the placement of the host site on the tilted face of PagP would decrease the ability of polar side chains to snorkel, the more favorable $\Delta\Delta G^{o}_{SC}$ in PagP compared to OmpLA seems to disprove this hypothesis. One way to increase the accessibility of side chains to the interface would be if the tilt of the PagP barrel were dynamic. Previous molecular dynamics studies of β-barrels have shown that the transmembrane domains can adopt a range of tilt angles with respect to the bilayer normal (8). PagP is known to be a "dynamic barrel" that can adopt multiple states and thus may be able to access a range of conformations with respect to the bilayer in thermal equilibrium (12,32). The addition of a polar residue at site 111 may change the average tilt angle to one that allows for more efficient side chain snorkeling to the interface. Additionally, this dynamic behavior of PagP could also serve to decrease the energy of creating lipid defects and allow for water dimple formation easier than OmpLA. Thus, we attribute the majority of the scaffold dependence of $\Delta\Delta G^{o}_{SC}$ to the general properties of the scaffold protein that dictate the ability of a side chain to reach a favorable chemical environment.

CONCLUSION

The energetics that govern membrane protein folding are linked to the burial of amino acid side chains in the hydrophobic lipid bilayer, which is theoretically independent of the protein sequence and structure. To investigate the validity of this assumption, we measured $\Delta\Delta G^{o}_{SC}$ in distinct scaffold proteins under the same experimental conditions for the first time, to our knowledge. We find that although many residues exhibited differences in $\Delta\Delta G^{o}_{SC}$ between measurements in PagP and OmpLA scaffolds, nonpolar residues, except valine and isoleucine, were found to be scaffold independent. This finding indicates that the protein scaffold affects $\Delta\Delta G^{o}_{SC}$ only when the side chain is placed in a noncompatible chemical environment and is forced to "snorkel" to a more favorable environment. The scaffold dependence therefore arises from the intrinsic properties of the scaffold protein and the bilayer that determine the energetic cost for side-chain snorkeling. Additionally, we found that the energy associated with proline-induced secondary structure disruption in PagP was very similar to those measured in α-helical membrane proteins. Together, these findings highlight the general applicability of our whole protein hydrophobicity scales to nonpolar residues in the center of the bilayer as well as the intricacies of side-chain snorkeling and packing that complicate the process. We hope these results, which are applicable to all membrane proteins, will aid the production of accurate algorithms for predicting membrane protein stabilities from both sequence and structure.

SUPPORTING MATERIAL

Two figures are available at http://www.biophysj.org/biophysj/supplemental/S0006-3495(17)30682-3.

AUTHOR CONTRIBUTIONS

D.C.M. and K.G.F. planned the overall strategy and wrote the manuscript. D.C.M. conducted and analyzed experiments and molecular dynamics simulations.

ACKNOWLEDGMENTS

We thank Hector Figueroa and Anne Rice for assistance in cloning the variants in this study, and Dr. Sarah McDonald and Dr. Patrick Fleming for experimental and computational guidance.

This work was funded by National Institutes of Health grants R01 GM079440 and T32 GM008403.

REFERENCES

1. Hong, H. 2014. Toward understanding driving forces in membrane protein folding. *Arch. Biochem. Biophys.* 564:297–313.
2. Tanford, C. 1978. The hydrophobic effect and the organization of living matter. *Science.* 200:1012–1018.
3. White, S. H., and W. C. Wimley. 1999. Membrane protein folding and stability: physical principles. *Annu. Rev. Biophys. Biomol. Struct.* 28:319–365.
4. Moon, C. P., and K. G. Fleming. 2011. Side-chain hydrophobicity scale derived from transmembrane protein folding into lipid bilayers. *Proc. Natl. Acad. Sci. USA.* 108:10174–10177.
5. Kroncke, B. M., A. M. Duran, …, C. R. Sanders. 2016. Documentation of an Imperative To Improve Methods for Predicting Membrane Protein Stability. *Biochemistry.* 55:5002–5009.
6. Moon, C. P., and K. G. Fleming. 2011. Using tryptophan fluorescence to measure the stability of membrane proteins folded in liposomes. *Methods Enzymol.* 492:189–211.
7. Moon, C. P., S. Kwon, and K. G. Fleming. 2011. Overcoming hysteresis to attain reversible equilibrium folding for outer membrane phospholipase A in phospholipid bilayers. *J. Mol. Biol.* 413:484–494.
8. Fleming, P. J., J. A. Freites, …, K. G. Fleming. 2012. Outer membrane phospholipase A in phospholipid bilayers: a model system for concerted computational and experimental investigations of amino acid side chain partitioning into lipid bilayers. *Biochim. Biophys. Acta.* 1818:126–134.
9. Snijder, H. J., I. Ubarretxena-Belandia, …, B. W. Dijkstra. 1999. Structural evidence for dimerization-regulated activation of an integral membrane phospholipase. *Nature.* 401:717–721.
10. Cox, K., and M. S. Sansom. 2009. One membrane protein, two structures and six environments: a comparative molecular dynamics simulation study of the bacterial outer membrane protein PagP. *Mol. Membr. Biol.* 26:205–214.
11. Cuesta-Seijo, J. A., C. Neale, …, G. G. Privé. 2010. PagP crystallized from SDS/cosolvent reveals the route for phospholipid access to the hydrocarbon ruler. *Structure.* 18:1210–1219.
12. Hwang, P. M., W. Y. Choy, …, L. E. Kay. 2002. Solution structure and dynamics of the outer membrane enzyme PagP by NMR. *Proc. Natl. Acad. Sci. USA.* 99:13560–13565.
13. McDonald, S. K., and K. G. Fleming. 2016. Aromatic side chain water-to-lipid transfer free energies show a depth dependence across the membrane normal. *J. Am. Chem. Soc.* 138:7946–7950.
14. Moon, C. P., N. R. Zaccai, …, K. G. Fleming. 2013. Membrane protein thermodynamic stability may serve as the energy sink for sorting in the periplasm. *Proc. Natl. Acad. Sci. USA.* 110:4285–4290.
15. Lomize, M. A., A. L. Lomize, …, H. I. Mosberg. 2006. OPM: orientations of proteins in membranes database. *Bioinformatics.* 22:623–625.
16. Jo, S., T. Kim, and W. Im. 2007. Automated builder and database of protein/membrane complexes for molecular dynamics simulations. *PLoS One.* 2:e880.
17. Jo, S., T. Kim, …, W. Im. 2008. CHARMM-GUI: a web-based graphical user interface for CHARMM. *J. Comput. Chem.* 29:1859–1865.
18. Brooks, B. R., C. L. Brooks, 3rd, …, M. Karplus. 2009. CHARMM: the biomolecular simulation program. *J. Comput. Chem.* 30:1545–1614.
19. Lee, J., X. Cheng, …, W. Im. 2016. CHARMM-GUI input generator for NAMD, GROMACS, AMBER, OpenMM, and CHARMM/OpenMM simulations using the CHARMM36 additive force field. *J. Chem. Theory Comput.* 12:405–413.
20. Wu, E. L., X. Cheng, …, W. Im. 2014. CHARMM-GUI membrane builder toward realistic biological membrane simulations. *J. Comput. Chem.* 35:1997–2004.
21. Khan, M. A., and R. E. Bishop. 2009. Molecular mechanism for lateral lipid diffusion between the outer membrane external leaflet and a β-barrel hydrocarbon ruler. *Biochemistry.* 48:9745–9756.
22. Bolen, D. W., and M. M. Santoro. 1988. Unfolding free energy changes determined by the linear extrapolation method. 2. Incorporation of ΔG° N-U values in a thermodynamic cycle. *Biochemistry.* 27:8069–8074.
23. Santoro, M. M., and D. W. Bolen. 1992. A test of the linear extrapolation of unfolding free energy changes over an extended denaturant concentration range. *Biochemistry.* 31:4901–4907.
24. Chothia, C. 1974. Hydrophobic bonding and accessible surface area in proteins. *Nature.* 248:338–339.
25. Eisenberg, D., and A. D. McLachlan. 1986. Solvation energy in protein folding and binding. *Nature.* 319:199–203.
26. Wimley, W. C., T. P. Creamer, and S. H. White. 1996. Solvation energies of amino acid side chains and backbone in a family of host-guest pentapeptides. *Biochemistry.* 35:5109–5124.
27. Elazar, A., J. Weinstein, …, S. J. Fleishman. 2016. Mutational scanning reveals the determinants of protein insertion and association energetics in the plasma membrane. *eLife.* 5:5.
28. MacArthur, M. W., and J. M. Thornton. 1991. Influence of proline residues on protein conformation. *J. Mol. Biol.* 218:397–412.
29. Yohannan, S., D. Yang, …, J. U. Bowie. 2004. Proline substitutions are not easily accommodated in a membrane protein. *J. Mol. Biol.* 341:1–6.
30. Humphrey, W., A. Dalke, and K. Schulten. 1996. VMD: visual molecular dynamics. *J. Mol. Graph.* 14:33–38, 27–28.
31. Hessa, T., H. Kim, …, G. von Heijne. 2005. Recognition of transmembrane helices by the endoplasmic reticulum translocon. *Nature.* 433:377–381.
32. Hwang, P. M., R. E. Bishop, and L. E. Kay. 2004. The integral membrane enzyme PagP alternates between two dynamically distinct states. *Proc. Natl. Acad. Sci. USA.* 101:9618–9623.
33. The PyMOL Molecular Graphics System, Version 1.8 Schrödinger, LLC.

Biophysical Journal, Volume *113*

Supplemental Information

Influence of Protein Scaffold on Side-Chain Transfer Free Energies

Dagen C. Marx and Karen G. Fleming

Supporting Information for:

Influence of Protein Scaffold on Side Chain Transfer Free Energies

D.C. Marx and K. G. Fleming

Table of Contents:

Figure S1. PagP site 111 experimentally determined side chain energy values for all twenty amino acids.

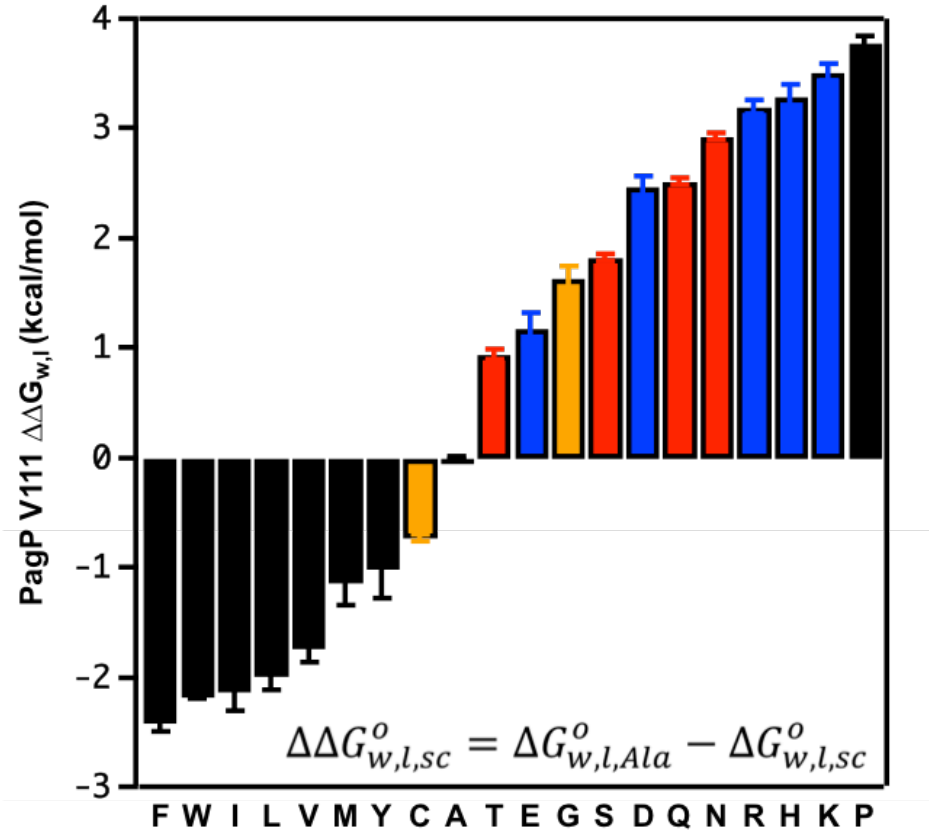

$\Delta\Delta G^{o}_{w,l}$ values were calculated by taking the difference in the stability of the V111A variant of PagP and V111X variant, where X is any amino acid (equation shown in figure). We find that most nonpolar residues are favorable at site 111 in PagP, except proline, which was the most unfavorable residue in the series. Polar residues were all unfavorable with respect to alanine, except cysteine. The coloring system is follows the same convention as Figures 2 and 5.

Figure S2. WT and V111P PagP molecular dynamics systems are equilibrated by 100 ns.

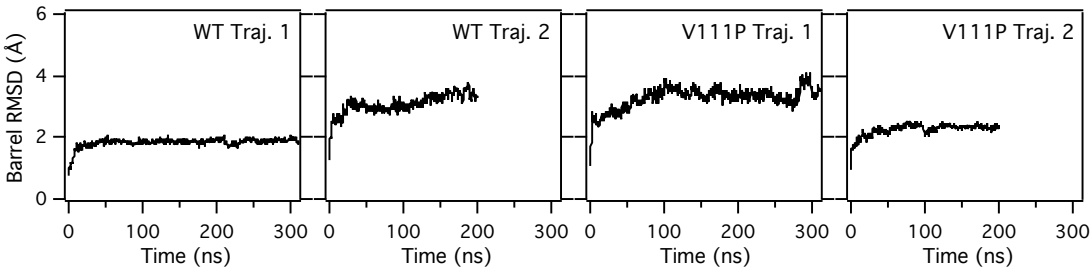

The RMSD (Å) compared to the starting structure of the backbone atoms are shown for all heavy atoms found in beta sheets. We find that all four trajectories equilibrated after 100 ns.